Magnetic Field Profiles Generated by a Solitary Propagating Action Potential via Hodgkin-Huxley Type Membrane Dynamics

Brett A. Sims †

Abstract

We generate magnetic field profiles via the simulation of one-dimensional action potential propagation in excitable tissue. Magnetic field profiles are produced by a solitary neural and cardiac traveling action potential. To accurately model experimental action potential morphology for neural and cardiac tissue, we used the Hodgkin-Huxley and Beeler-Reuter equations respectively. We study and compare several simulated magnetic field profiles computed at specified distances from the theoretical tissue in which the action potential is propagating. The analysis of the magnetic fields in this forward problem reveals signatures of neural and cardiac electrical behavior. Our simulated results suggest that experimental magnetic field studies can be used to, non-invasively, determine electrical behavior in excitable tissue at the cellular level.

1. Introduction

Over the last two decades noninvasive techniques have been used to study electrical activity in excitable tissue. In the field of biomagnetism, a particular approach is to measure the magnetic field near the body, organ, or tissue, and determine the electrical sources within the tissue that produced the measured magnetic field. Mathematically, this poses an inverse problem, that is, given a magnetic field profile, determine the electrical sources and activity that produced the magnetic field. Basic questions that could be answered by the study of neural- or cardio-magnetism involve the determination of ectopic foci and tissue electrical properties (conductance, branching, or capacitance). Determining the electrical distributions responsible for the magnetic field is a difficult inverse problem. There are many different techniques that can be used to solve the inverse problem, for instance the least-squares method or Signal Space Projection analysis [1, 2]. In 2004, Amblard et al [3] studied biomagnetic source detection of distributed current sources on the cortical surface. Via an ill-posed inverse problem addressed with in the frame work of the maximum entropy on the mean principal, they employed a regularization technique using a reference probability measure on random variables- Markov in nature- that quantify the intensity of current sources. However, there are many different electrical source distributions that can produce the same magnetic field profile.

In this study we employ the forward problem, that is, the computation of magnetic field profiles generated by a known propagating action potential.

The forward problem plays an important role in the investigation and comparison of computed magnetic field profiles to identify signatures of electrical activity found in its associated magnetic field. The Hodgkin-Huxley [4] equations for neural tissue and Beeler-Reuter [5] equations for cardiac tissue have accurately modeled the experimental results for the action potential in neural and cardiac tissue. To accurately simulate the one-dimensional propagating action potential in neural and cardiac tissue we used the one-dimensional reaction-diffusion equation, incorporating the Hodgkin-Huxley and Beeler-Reuter equations respectively. Magnetic field strength profiles were computed using the Biot-Savart law involving intracellular current only. The extracellular current and membrane current were not computed since their contribution to the magnetic field strength is negligible [6, 7].

In 1996, Brio and Marchesin outlined a first step in their study of wave propagation in myocardial tissue [6]. They modeled two-dimensional action potential propagation via the reaction diffusion equation with FitzHugh-Nagumo [8] type and piecewise linear membrane dynamics. FitzHugh-Nagumo and piecewise linear type membrane dynamics provide for a more qualitative investigation of the action potential and its propagation than the Hodgekin-Huxley type membrane dynamics. However, the former does not provide for a detailed study of the contribution of individual species of ionic membrane currents to the action potential morphology and its propagation. Further, FitzHugh-Nagumo and piecewise linear type membrane dynamics produce action potential morphologies that are different from experimental data for excitable tissue.

Recent modeling practices for computing biomagnetic fields are based on current dipoles and current dipole densities. Nervat et al [9], in 2004, applied a forward problem model that generated magnetic field profiles via electric dipole conduction in a theoretical head (brain and skull) model. They studied the sensitivity of simulated magnetic field recordings to perturbations in conduction of the head. In 2006, Wolfgang et al [10] computed magnetic field vectors via current density maps. Current density is taken to be a three dimensional distribution of electric dipole currents. While the modeling of biomagnetic fields via electric dipole current distributions allow for a qualitative study of biomagnatic fields and their sources, the current dipole does not relate the magnetic field to the action potential as a source, nor do current dipoles provide a means to study the biomagnetic field sensitivity to perturbations in specific ionic membrane currents. Magnetic fields produced by Hodgkin-Huxley type membrane dynamics allow for the detailed study of the influences of the action potential phases on the magnetic field morphology.

In this paper, we compute the solution (action potential) to the reaction-diffusion equation with a Hodgkin-Huxley type source term. The magnetic field is computed via an intracellular current that is a direct function of the action potential.

2. Method

The Model

A reaction diffusion equation was derived from a theoretical one-dimensional fiber represented by a myocyte chain, see Figure 1. The biological environment of the myocyte chain in Figure 1 was quantified electrically where V_e and V_i are the extra- and intracellular potential respectively, I_e and I_i are the extra- and intracellular current respectively, and membrane current $I_m = I_c + I_{ion}$ is the sum of capacitive current and ionic currents. Here, we assumed that the extracellular potential V_e is constant and that the electrical quantity for resistance of the extracellular environment is negligible in comparison to that of the intracellular invironment. We also assume that the cell membrane has a dielectric property and contributes a membrane capacitance to the bioelectric environment.

Kirchoff's current and voltage laws were used to derive a one-dimensional reaction diffusion equation to model action potential propagation, Equation 1,

$$C_m \frac{\partial V_m}{\partial t} = \frac{1}{R_i} \frac{\partial^2 V_m}{\partial x^2} + I_{ion}, \qquad (1)$$

where $V_m = V_i - V_e$ is the membrane voltage, R_i is the intercellular resistance (constant), I_{ion} is the ionic current, and C_m is the membrane capacitance (constant). The left hand term describes the capacitive current through the membrane and the first term on the right hand side describes the change in the intercellular current.

The Crank-Nicholson method was used to numerically compute the traveling wave solutions $V_m(x,t)$ for equation (1). Hodgkin-Huxley [4] and Beeler-Reuter [5] membrane dynamics were used for the source term I_{ion} in the computation of the traveling neural and cardiac action potentials respectively.

Spatial and Time stepping Grid

The spatial domain is a one-dimensional theoretical fiber of length L with Dirichlet boundary conditions and has a uniform grid containing N grid points. Suitable piece-wise linear distributions were used for the initial condition $V_m(x,0)$. The grid spacing is $\Delta x = L/N$. The Laplacian $\partial^2 V_m / \partial x^2$ was computed at the midpoint grid element Δx. The diffusion coefficient used in the computation is λ^2/τ where the space and time constants are

$$\lambda = \sqrt{\frac{R_m d}{4\rho_c}} \text{ and } \tau = R_m C_m$$

respectively. The membrane resistance is R_m, d is the cell diameter, ρ_c is the cytoplasmic resistivity, and C_m is the membrane capacitance. Parameters for the time and space constants are found in [11].

The scheme for time stepping involves the L_∞ norm of a weighted Jacobian of the source term [11]. For each time step, Δt was computed to prevent numerical instabilities and maintain the quality of the fast action potential rising phase and very large derivatives of the action potential. All computations were performed on a LINUX computer.

Magnetic Field Strength Computation

The Biot-Savart law was used to calculate the magnetic field strength $H(t)$ at a distance r from the one-dimensional fiber conducting the propagating action potential, equation (2). Integral equations for the Biot-Savart law were numerically computed using the midpoint rule where the intracellular current $I_i = V_m / R_i$ is a function of the action potential.

$$H = \frac{1}{4\pi} \int \frac{I_i \times \hat{r}}{r^2}. \qquad (2)$$

Results

Neural Action Potential and Magnetic Field Profiles

Illustrated in Figure 2 is the typical neural action potential reproduced by the Hodgkin-Huxley equations. We simulated the one-dimensional propagation of the neural action potential in figure 2 via equation 1 and used its spatial-temporal distribution, $V_m(x,t)$ to produce magnetic field strength profiles. The neural action potential exhibits three phases- the rising phase from -60 mv to a 10 mv peak in approximately 1ms, the falling phase from 10 mv to -100 mv in approximately 3 ms and the hyperpolarization phase from -100 mv to -90mv in approximately 15 ms. The derivatives of the rising and falling phases are on the order of 10 mv/ms and are very large relative to the derivative of the hyperpolarization phase, which is on the order of about 1 mv/ms.

Figures 3 – 6 illustrate the time transient of the magnetic field strength magnitude computed at positions (x,y) along the one-dimensional fiber where x, in centimeters, is the distance on the fiber from the beginning of the fiber and y, in centimeters, is a length perpendicular to the fiber. The magnetic field strength is in $\mu A/cm$. Each time transient magnetic field strength profile was computed for the duration of its neural action potential propagation simulation.

It is known that the greatest contribution to the magnetic field is due to the relatively large derivatives of the traveling action potential and the significant axial current I_i that it produces. For the neural action potential these large derivatives occur during the rising phase and falling phase of the action potential. In Figure 2 the rising and falling phases, together, last for approximately 4ms and we expect significant axial currents during these phases. Note that the hyperpolarization phase of Figure 2 lasts for a duration of approximately 15 ms where the derivative of the action potential is significantly less than the derivatives of the rising and falling phases. We expect that axial currents produced by the hyperpolarization phase will be significantly less than axial currents produced by the rising and falling phases.

In Figure 3 the magnetic field strength was computed at a theoretical position (2.25, 1) and produced by a traveling neural action potential traveling in a straight line. The two maxima in the magnetic field strength are a result of axial currents produced by large derivatives, rising and falling phases. Also note two minima, the first produced by the zero derivative action potential peak and the second minimum produced by the small derivative of the action potential repolarization phase. Figure 4 is the magnetic field strength computed at the position (2.25, .25). The peak-to-peak distances in magnetic field strength in Figure 4, on the order of hundreds of micro amps per centimeter, are larger in magnitude than the peak-to-peak magnitudes shown in Figure 3, order 10 $\mu A/cm$. The computation for Figure 4 was taken at a position closer to the current conducting fiber, .25cm, than the computation for Figure 3, computed at a distance of 1cm from the fiber. An artifact, the small -700 $\mu A/cm$ peak, in Figure 4 is a result of a perturbation at the on-set of the action potential simulation.

The magnetic field strength illustrated in Figure 5 was computed at the position (2.24, 4). Computation of the magnetic field at a position further away from the conducting fiber, at 4cm, produced peak to peak magnitudes in the magnetic field strength that are on the order of a micro amp per centimeter - significantly less than peak-to-peak magnitudes found in Figures 3 and 4. There are three maxima and two minima in the magnetic field strength of Figure 5. In the upper left-hand corner of

Figure 5 the grouped magnitudes of the first two maxima are approximately 1 $\mu A/cm$ apart in magnitude, with a local minimum, between, whose magnitude is
1 $\mu A/cm$ apart from the second maximum. At a distance of 4cm from the conducting fiber, that point experiences the net contribution of the high derivatives of the rising and falling phases of the action potential, the result is the grouped extrema illustrated in Figure 5. For the magnetic fields computed at positions closer to the conducting fiber, illustrated in Figures 3 and 4, the individual contributions of the large derivatives of the rising and falling phases are observed.

Figure 6 illustrates the magnetic field strength computed at the point (5, .25). Here, the magnetic field strength maximum occurs 40ms after the start of the action potential propagation simulation indicating that the action potential pulse took 40ms to travel 5cm. In Figure 4 the magnetic field strength maximum occurs 20 ms after the start of the action potential propagation simulation indicating that the action potential pulse took 20 ms to travel 2.25 cm. The velocity of the propagating action potential is 1.125 m/s in the simulations for Figures 4 and 6, which is in the range of action potential velocities for Purkinje fibers and skeletal muscle fibers, 1 m/s and 6 m/s respectively [12]. In Figures 3 – 6 note the small global minimum in the magnetic fields produced by the relatively small derivative of the hyperpolarization phase of the neural action potential.

Figure 7 illustrates the magnetic field strength computed at the point (2.25, 1) and produced by the propagation of two neural action potentials beginning at opposite ends of the conducting fiber and colliding. The magnetic filed profile reveals that the two action potentials overlap at the position 2.25cm. In terms of peak-to-peak temporal magnitudes and morphology, the magnetic filed profile of Figure 7 is similar to that of Figure 3, except for several cusps in the graph of Figure 7. This suggests that the overlapping neural action potential produced a net time varying neural action potential, $V_{net}(2.25,t)$, at position 2.25cm. Note the cusps in the magnetic field profile at approximately 2ms, 32ms, and 35ms after the start of the simulation. The cusp at 35ms yields a minimum. The cusps in the magnetic field profile at position (2.25, 1) for the indicated times suggests that there were jump or infinite discontinuities in $V_{net}(2.25,t)$ at position 2.25cm, for those respective times. We rule out infinite discontinuity in the morphology of $V_{net}(2.25,t)$since the simulation is discrete and finite in nature.

The overlapping action potential simulation in this paper is an extension of and corroborates with a discussion of the biological effects of overlapping and non-overlapping action potentials, found in Silverthorn [13]. The discussion in the human physiology text by Silverthorn considers two cases for general types of action potential interaction. In one case two subthreshold action potentials reach a position on a neuron- one after the other. The time interval between the two subthreshold action potentials is sufficiently long so that the two action potentials do not overlap and there is no net action potential produced at the position in question. The second case considers two subthreshold action potentials that do overlap at a position on a neuron and have a summation effect to produce a net action potential at the position in question.

Cardiac Action Potential and Magnetic Field Profiles

Illustrated in Figure 9 is the typical cardiac action potential reproduced by the Beeler-Reuter equations. We simulated the one-dimensional propagation

of the cardiac action potential in figure 9 via equation 1 and used its spatial-temporal distribution, $V_m(x,t)$ to produce magnetic field strength profiles. The cardiac action potential exhibits tree phases- the rising phase from -80 mv to a 20 mv peak in approximately 10ms, the plateau phase from a 20 mv peak to 5 mv in approximately 68 ms, and a falling phase from 5 mv to -80 mv in approximately 100 ms. The derivative of the rising phase is on the order of 10 mv/ms and is very large relative to derivatives of the other two phases. The derivative of the plateau phase is on the order of .1 mv/ms and the falling phase is on the order of 1 mv/ms. The relatively small derivative of the plateau phase suggests its name.

Figures 10 – 12 illustrate the time transient of the magnetic field strength magnitude computed at positions (x,y) along the one-dimensional fiber where x, in centimeters, is the distance from the beginning of the fiber and y, in centimeters, is a length perpendicular to the fiber. Distances are in centimeters and magnetic field strength is in $\mu A/cm$. Each time transient magnetic field strength profile was computed for the duration of its cardiac action potential propagation simulation.

We expect that the greatest contribution to the magnetic field will be due to the relatively large derivatives of the traveling cardiac action potential and the significant axial current I_i that it produces. For the cardiac action potential the large derivative occurs during the rising phase, about 10 ms in duration. The derivative of the plateau is negligible and falling phase derivative small, relative to the rising phase. We expect that axial currents produced by the plateau and falling phases will be significantly less than axial currents produced by the rising phase.

All magnetic field profiles in Figures 10 – 12 exhibit one maximum that reflects the strong axial current produced by the large rising phase derivative. Two maxima, as exhibited in the magnetic field profiles generated by the traveling neural action potential, are not present in the magnetic fields generated by the traveling cardiac action potential. The difference in the magnitudes of the magnetic fields depicted in Figures 10 – 12 reflect the difference in the distances from the conducting fiber, at which, the magnetic fields were computed. Magnetic fields for Figures 10, 11, and 12 were computed at (2.25, 1), (2.25, .25), and (2.25, 4) respectively. The magnetic field in Figure 11 computed at (2.25, .25) exhibits the greatest magnitude. The magnetic field in Figure 12 computed at (2.25, 4) exhibits the smallest magnitude with the magnetic field in Figure 10 being intermediate in magnitude. The morphology of the magnetic field computed nearer the conducting fiber, Figure 11, closely resembles the morphology of the cardiac action potential in Figure 9. The magnetic field in Figure 10 has a relatively narrow morphology and the magnetic field profile in Figure 12 exhibits a relatively broad morphology.

Figure 13 depicts the time transient of the magnetic filed strength at a position (-2.25, 2.25, 1) produced by a cardiac action potential traveling on a circular path centered at the origin. The circle has radius $5/\pi\, cm$ and x, y, and z coordinates are in centimeters with the x-y coordinates in the plane of the circle and the z coordinate above the circular plane. Point
(-2.25, 2.25, 0) is on the circle. At the on-set of the magnetic field time transient in Figure 13 there is a maximum. From approximately 150 ms to 300 ms the magnetic field is near its minimum. At 450 ms the magnetic field returns to its maximum. The profile of the magnetic field allows us to track the location of the rising phase of the cardiac action potential as the action potential travels around the circle. The magnetic field maximum at $t = 0$ ms indicates that the rising phase was at the position (-2.25, 2.25) on the circle. From approximately 150 ms to 300 ms the action potential rising phase was at a position on the circle sufficiently far from the point (-2.25, 2.25), which is reflected in a minimized magnetic field at the point (-2.25, 2.25, 1). In 450 ms the rising phase of the action potential returns to the position (-2.25, 2.25), reflected by a maximum in the magnetic field. The circumference of the action potential path is 10 cm which suggests that the action potential traversed its path in approximately 450 ms. The speed of the cardiac traveling action potential is approximately .222 m/s.

The average speed of the propagating cardiac action potentials, computed from data in Figures 10 – 13, is 0.46 m/s, which is near that of the cardiac action potential speed for cardiac muscle, 0.5 m/s [12].

Conclusion

This paper presented various magnetic field profiles produced by the simulation of a solitary one-dimensional traveling action potential, cardiac and neural. The time transient morphology for both the cardiac and neural action potentials in our simulations are biologically accurate. Further, the propagation speeds of the simulated traveling action potentials are near to the speeds of experimentally measured action potentials for neural and cardiac tissue. The magnetic field profiles in this paper have not been verified experimentally; however, the biological soundness of the traveling action potential simulations performed in this research informs us on how to investigate magnetic behavior at the cellular level. These simulations may be applied to the study of biomagnetic fields produced by the action potential propagation across boundaries between different types of excitable tissue. Also, for various branching systems, magnetic field detection at branching points may be investigated.

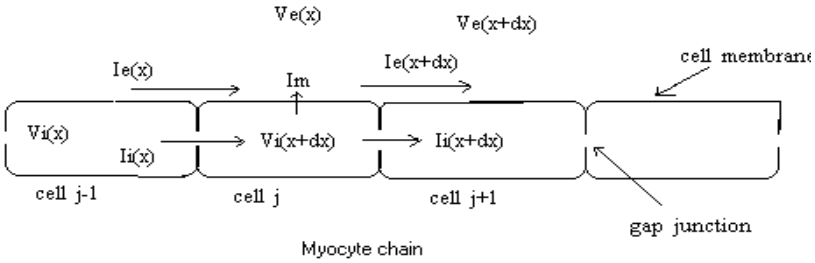

Figure 1. Myocyte Chain. A one-dimensional fiber connected end to end via gap junctions.

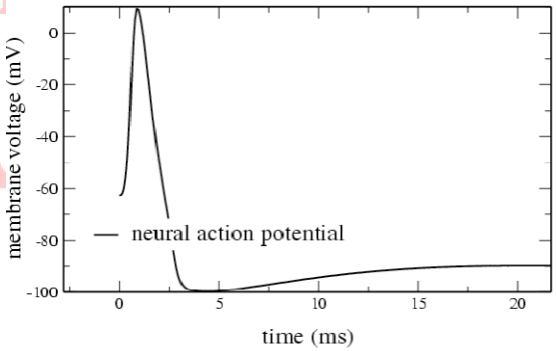

Figure 2. The time course for the neural action potential. Membrane voltage (mV) vs. time (ms).

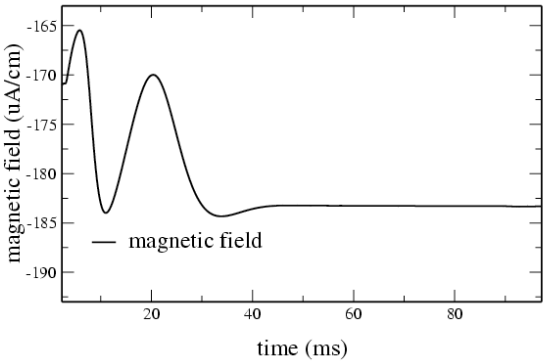

Figure 3. Magnetic field strength $(\mu A/cm)$ vs. time (ms) measured at position (2.25, 1) (cm) produced by a neural action potential traveling in a straight line.

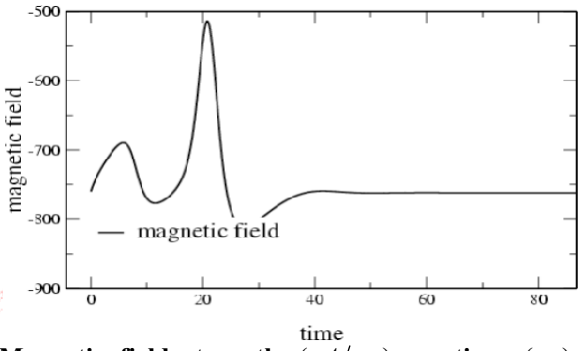

Figure 4. Magnetic field strength $(\mu A/cm)$ **vs. time** (ms) **measured at position (2.25, .25)** (cm) **produced by a neural action potential traveling in a straight line.**

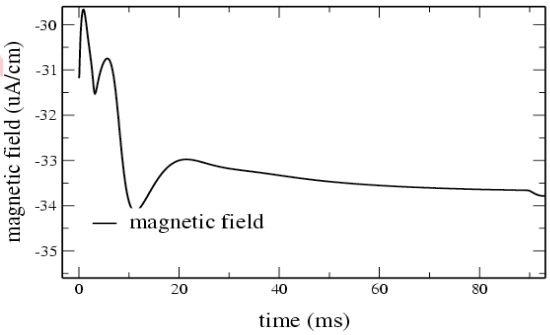

Figure 5. Magnetic field strength $(\mu A/cm)$ **vs. time** (ms) **measured at position (2.25, 4)** (cm) **produced by a neural action potential traveling in a straight line.**

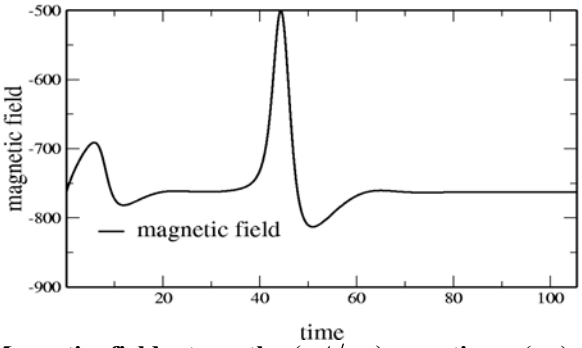

Figure 6. Magnetic field strength $(\mu A/cm)$ **vs. time** (ms) **measured at position (5, .25)** (cm) **produced by a neural action potential traveling in a straight line.**

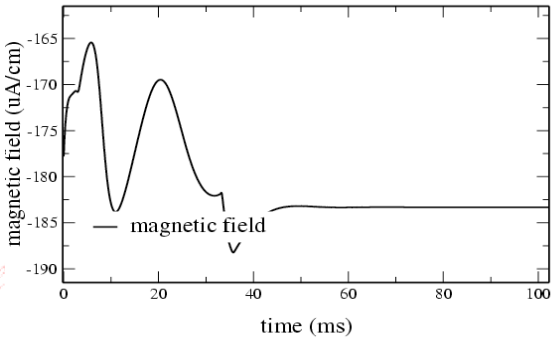

Figure 7. Magnetic field strength $(\mu A/cm)$ **vs. time** (ms) **measured at position (2.25, 1)** (cm) **produced by two neural action potentials traveling towards each other in a straight line and colliding.**

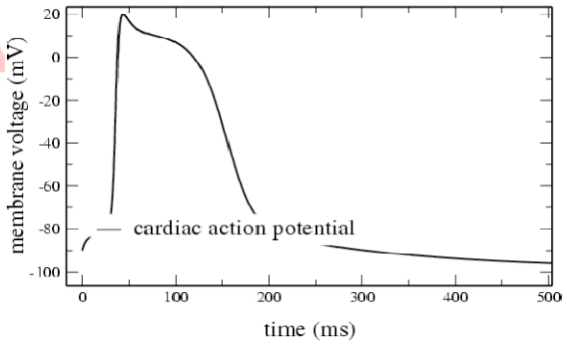

Figure 9. The time course for the cardiac action potential. Membrane voltage (mV) **vs. time** (ms)**.**

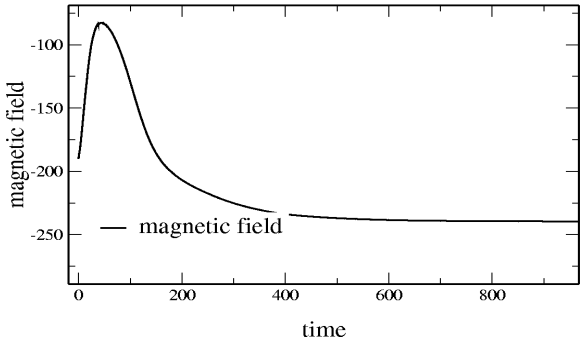

Figure 10. Magnetic field strength $(\mu A/cm)$ **vs. time** (ms) **measured at position (2.25, 1)** (cm) **produced by a cardiac action potential traveling in a straight line.**

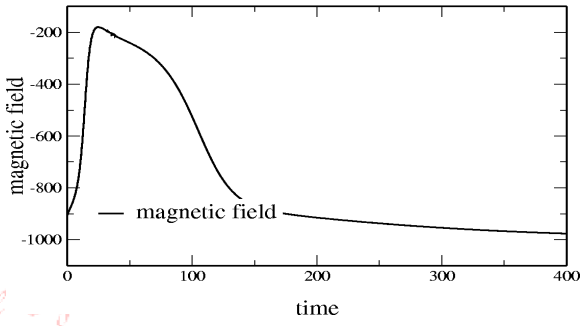

Figure 11. Magnetic field strength $(\mu A/cm)$ **vs. time** (ms) **measured at position (2.25, .25)** (cm) **produced by a cardiac action potential traveling in a straight line.**

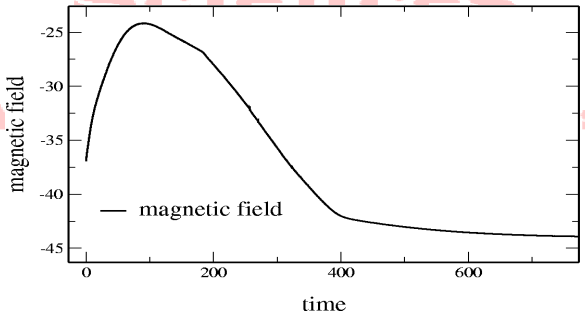

Figure 12. Magnetic field strength $(\mu A/cm)$ **vs. time** (ms) **measured at position (2.25, 4)** (cm) **produced by a cardiac action potential traveling in a straight line.**

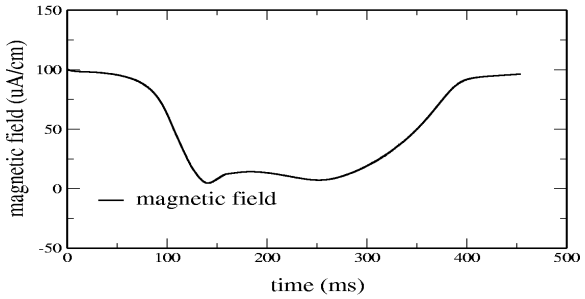

Figure 13. Magnetic field strength $(\mu A/cm)$ **vs. time** (ms) **measured at position (-2.25, 2.25, 1)** (cm) **produced by a cardiac action potential traveling on a circular path of radius** $5/\pi\, cm$ **centered at the origin.**

† *Brett A. Sims, Ph.D., Grambling* State University, Louisiana, USA

References

[1] C. D. Tesche, M. A. Uusitalo, R. J. Ilmoniemi, M. Huotilainen, M. Kajola, and O. Salonen. Signal-space projections of MEG data Characterized by both distributed and well-localized neuronal sources. Electroencephalography and Clinical Neurophysiology, 95: 189-200, 1995.

[2] Matti S. Hamalainen. Functional Localization based on measurements with a whole-head magnetometer system. Brain Topography, 7:283-289, 1995.

[3] C. Amblard, E. Lapalme, T. Lina. Biomagnetic source detection by maximum entropy and graphical models. IEEE Transactions on Biomedical Eng, Volume 51, Issue 3, pgs 427-442, 2004.

[4] A. L. Hodgkin and A. F. Huxley. A quantitative description of membrane current and its application to conductance and excitation in nerve. J. Physiol., 117:500-544, 1952.

[5] G. W. Beeler and H. J. Reuter. Reconstruction of the action potential of ventricular myocardial fibers. J. Physiol., 268:177-210, 1977.

[6] M. Brio and Dan Marchesin. Evolutionary bidomain model of continuous excitable medium. Mathematica Contemporanea, 10:75-86, 1996.

[7] J. P. Wikswo. S. J. Williamson et al., editor, Advances in Biomagnetism: Biomagnatic Sources and Their Models. Plenum Press, New York, 1989.

[8] R. FitzHugh. Impulses and physiological states in theoretical models of nerve membrane. Biophysical Journal, 1:445-466, 1961.

[9] N. Gencer et al. Sensitivity of EEG and MEG measurements to tissue conductivity. Phys. Med. Biol., 49:701-717. 2004

[10] Wolfgang Haberkorn et al. Pseudo current density maps of electrophysiological heart, nerve, or brain function and their physical basis. Biomagnatic Research and technology, 4:5. 2006.

[11] B. Sims. Action potential propagation in myocardial tissue. PhD Thesis, SUNY Stony Brook, NY. Pgs 48-51. 2002

[12] J. Keener and J. Sneyd. Mathematical Physiology. Springer-Verlag, New York-Heidelberg-Berlin, 1998.

[13] D. Silverthorn. Human Physiology An Integrated Approach. Prentice-Hall Inc, NJ, 1998.